nature nanotechnology

SUPPLEMENTARY INFORMATION

DOI: 10.1038/NNANO.2009.311

Self-assembly of Carbon Nanotubes into Two-dimensional Geometries using DNA Origami Templates

Hareem T. Maune Si-ping Han Robert D. Barish Marc Bockrath
William A. Goddard III Paul W.K. Rothemund Erik Winfree

S1 Formation of and purification of NL-SWNTs

Design and formation of the linker complex. Oligos were purchased in lyophilized form from IDT DNA. Sequences are below. LNA nucleotides are written as +C+G+A, etc. All other nucleotide are DNA. Labeling domain sequences were computer-optimized (*31*) to minimize sequence complementarity, homology, and melting temperature differences with programs written in MATLAB available at:

`http://www.dna.caltech.edu/DNAdesign/`

Red linker main strand:
`5′ TTTTTTTTTTTTTTTTTTTTTTTTTTTTTTTTTTTTTTTTTTGTTGCGAGGTCTTGC+C+G+A+C+A 3′`
Red linker protection strand:
`5′ GCAAGACCTCGCAAC 3′`
Blue linker main strand:
`5′ TTTTTTTTTTTTTTTTTTTTTTTTTTTTTTTTTTTTTTTTTTATACGGGGCTGGTTA+G+G+A+T+G 3′`
Blue linker protection strand:
`5′ TAACCAGCCCCGTAT 3′`

Strands are separately dissolved in water purified by a Milli-Q unit (Millipore) to form stock solutions at $\sim$300 μM. A 2 M NaCl stock solution is created and filtered using 0.22 μm filters. For the red (blue) linker complex, the main strand and the protection strand are mixed with NaCl stock solution and Milli-Q purified water to obtain 600 μL of dispersal solution with $\sim$ 33 μM of the main strand, $\sim$ 36 μM of the protection strand, and 0.1 M NaCl; the concentrations of the main and protection strands were chosen to give a 10% excess of protection strand. This solution is put in a 0.6 mL PCR tube and annealed in an Eppendorf Mastercycler from 95°C to 20°C at 1°C per minute. The protection strand/main strand partial duplex has a melting temperature $T_{melting}$ $\sim$50°C in our buffers.

Dispersal of SWNTs. To create the red (blue) NL-SWNTs, $\sim$1 mg of dry HiPco SWNTs are added to 400-600 μL of the dispersal solution in a 1.7 mL PCR tube. The tube is then placed in an ice-water bath and sonicated for $\sim$90 minutes in a Branson 2510 sonicator (100 W). The water level inside the sonication chamber and the position of the PCR tube is adjusted to apply maximum sonication power to the sample. The temperature of the water bath is maintained at $\sim$15 °C. The SWNTs are sonicated until the solution turns a uniform gray color and all the SWNTs are completely solubilized. The solution is then centrifuged at 16,000 g for 90 min at 15°C. Following this step, the supernatant is retained while the insoluble condensate is discarded. This process yields a high concentration of well-dispersed NL-SWNTs as determined by AFM and TEM images.

DOI: 10.1038/NNANO.2009.311

Removal of excess linker complexes. The dispersal procedure for creating NL-SWNTs leaves a large excess of free linker complexes in solution that needs to be reduced before self-assembly. We apply electrodialysis using a Harvard Apparatus Electroprep system. A 500 μL Teflon fast dialysis tube is filled with NL-SWNT solution and capped at both ends with 50 kD MWCO cellulose ester dialysis membranes. The dialysis tube is then placed in the Electroprep tank. The tank is filled with 0.1 M Na_2HPO_4 buffer (filtered with a 0.22 μm membrane).

A constant current of 15 to 20 mA is applied across the electrodes of the Electroprep tank. The current is run for 2 hours. The electrodes are then disconnected and the tank is washed. Fresh buffer is added, the direction of the dialysis tube is reversed such that the membrane facing the cathode now faces the anode, and the current is run for another two hours. Buffer exchange and current reversal are repeated two more times before retrieving the NL-SWNT solution (8 hours total of electrodialysis).

To retrieve the NL-SWNTs, the capped dialysis tube is washed using Milli-Q purified water. It is placed in a beaker with 0.1 M Na_2HPO_4 buffer and ultra-sonicated for 30 seconds to 1 minute in a Branson 2510 sonicator. This releases any NL-SWNTs stuck on the membranes back into the solution contained inside the dialysis tube. The tube is then uncapped and the purified NL-SWNT suspension is recovered using an appropriate pipette.

The UV absorbance at 260 nm is measured and compared to the absorbance of an unfiltered NL-SWNT sample. We find that the self-assembly of NL-SWNTs on DNA origami is most efficient when the UV absorbance of the purified solution at 260 nm is $< 5\%$ of that of the initial solution. If the UV absorbance is higher, or if assembly efficiency is poor, electrodialysis is repeated with fresh filter membranes and buffer. We usually repeat the 8 hour dialysis process three times on the same sample. Immediately after purification, NL-SWNT solutions are divided into 50 μl aliquots and stored in a -80°C freezer where they are stable for months. Room temperature storage or 4°C storage causes aggregation and decreased binding to origami after a few days; -20°C might afford stability for weeks or months but we have not made a systematic study of NL-SWNT stability as a function of storage temperature.

The method we used to determine the stopping point for purification only addresses the decrease of the excess linker and does not address the ratio of excess free linker to linkers bound to the SWNTs, which is the more important measure since it determines whether the remaining excess of free linkers is so high that it saturates the hooks on the origami and prevents NL-SWNTS from binding to origami. Thus we used gel-electrophoresis to evaluate this ratio for some batches of NL-SWNTs.

Non-denaturing polyarylamide gel electrophoresis (ND-PAGE) is used to estimate the amount of free linker DNA. Free linkers migrate into the gel where they may be quantified, while bound linkers remain stuck on the carbon nanotubes that do not migrate from the well. We use 8% or 10% polyacrylamide (polymerized by 1% by volume of 10% ammonium persulfate (APS) and cross-linked by 0.075% by volume tetramethylethylenediamine [TEMED]) in a 1× TAE/Mg^{2+} buffer (40 mM Tris-acetate, 1 mM EDTA, 12.5 mM magnesium acetate, pH 8.3). A constant field of 8 V/cm is applied across the gel (80 V, 10 cm length, I∼34 mA, 1 mm thick mini-gel) for 3-4 hours while the buffer temperature is kept at 15°C. A 10 base pair ladder (Invitrogen) is used in one of the gel lanes as a length reference. A lane of free linker complexes is included to allow quantitation. Finally, the gel is stained with Sybr Gold (Invitrogen) for 25 minutes and imaged using a Bio-Rad Molecular Imager FX.

Denaturing PAGE (8%, 7 M urea, 175 V, 17.5 V/cm, 60°C, stained similarly to ND-PAGE) was used to estimate the total amount of linker DNA in the sample after the electrodialysis procedure. The idea is that strong denaturing conditions and high temperature* detach the linkers from the nanotubes, so that

*Here a field strength of 17.5 V/cm seemed to be more effective at detaching linkers than 8 V/cm. This could have been caused incidentally by greater heating, or perhaps the somewhat elevated field played a direct role since the carbon nanotubes do not migrate in the gel and are not free to move with the linkers.

the total can be measured. From the total and the free linker concentration, we estimate the amount of linker bound to the carbon nanotubes ($\mathrm{bound} = \mathrm{total} - \mathrm{free}$).

The amount of free and SWNT-bound linkers varies between different preparations of NL-SWNTs; bound linker typically ranged from $\sim$ 100 nM to 1 μM. As a specific example, for the batch of blue SWNTs used in Fig. 2, we estimated that the concentration of linker bound to SWNTs was 420 nM and the concentration of free linker was 120 nM, even after it had undergone a few freeze thaw cycles (and been used in successful experiments). This represents a free:bound linker ratio of $\sim$1:3. If the ratio is too high, then presumably free linker will bind all hook sites and prevent SWNTs from binding. Because NL-SWNTs bind origami at multiple sites, some poisoning of these sites by free linker may be tolerated. We have not explored the highest ratio of free:bound linker that is acceptable.

DOI: 10.1038/NNANO.2009.311

S2 Design, assembly, and purification of the DNA template

Tall rectangle origami templates. The DNA origami used in our experiments is a modified version of the "tall rectangle" designed by Rothemund (Supplementary Information Figs. S36 and S48 in (*20*)). The sequences for the original origami are shown in Fig. S48 of (*20*). We modified the origami as shown in Fig. S1. Specifically, we replaced particular DNA staples with the strands listed in Figs. S2 and S3. Their names, listed in the "Position and sequence" columns, correspond to the names of the original staples shown in Rothemund's Fig. S48 (*20*)but have "FHook1" or "FHook2" added. In general their sequences differ from the original staples by the addition, on the 3' end, of (1) a 4 thymine flexible linker and (2) an appropriate hook sequence.

The linker + red hook sequence is:
`5′ TTTTTGTCGGCAAGACCTCGCAAC 3′`
This corresponds to the red linker sequence:
`5′ GTTGCGAGGTCTTGCCGACA 3′`

The linker + blue hook sequence is:
`5′ TTTTCATCCTAACCAGCCCCGTAT 3′`
This corresponds to the blue linker sequence:
`5′ ATACGGGGCTGGTTAGGATG 3′`

The staples which are used for the blue column of hooks are actually not quite simple catenations of original staples with the linker and blue hook sequence. The domain by which these staples bind the origami scaffold strand is actually shifted 5 nucleotides with respect to the binding domain which is used for the original staples—this can be observed in Fig. S1. It means that (1) the scaffold binding domain of each staple in the blue column is actually a composite of two staples in the same column in the original origami, 5 nucleotides from one staple and 27 nucleotides from another and (2) one of the sequences (t1r0g-FHook2) does not actually bear a blue hook—instead it is a staple on the top edge of the origami that had to be modified to accomodate the shift in strand ends implied by (1).

Origami-nucleated DNA/ribbon templates. We created a larger DNA template from the DNA origami by growing a periodic structure from the edge of the DNA origami using DNA tiles. The structures, known as zig-zag ribbons, were first described in (*34*) and their nucleation and growth from origami was shown in (*35*). The DNA tiles constituting the ribbon are each made from four single DNA strands: two long strands (37 nt) and two short strands (26 nt), which displaying 5-base sticky ends for binding with other tiles. A schematic for a tile attached to the origami is present at top, in Fig. S1. Tiles comprise of just two DNA helices and are much smaller ($\sim$12 nm$\times$4 nm) than a DNA origami ($\sim$ 95 nm $\times$ 75 nm), but they can assemble into a much larger periodic ribbons, which are typically from 4-16 tiles wide and hundreds of tiles long. The long edge of the tall rectangle origami has 32 helices, so up to 16 DNA tiles can be fit onto the edge of the origami by using a set of adapter strands (*35*). Here we used 16-tile wide ribbons everywhere except for an experiment documented by Fig. S5d,h which used an 8-tile wide ribbon. Because the origami forms at higher temperatures than the assembly of tiles into zig-zag ribbons, origami serve as good nuclei for the growth of zig-zag ribbons—a cooled mixture of their component strands forms products that are almost entirely composed of DNA origami with crystalline zig-zag ribbons grown from their edge. The resulting ribbons are $\sim$100 nm wide and typically 500 nm to 1 μm long.

Ribbons coupled to origami are a highly visible marker for the orientation of the DNA origami (red face up or blue face up), even when imaging resolution is low. Patterns of hairpins on the DNA origami could have served to disambiguate orientation, but experiments analysis would have been much more challenging since they require higher resolution imaging. Qualitatively, more SWNT/DNA template structures were observed post-assembly when DNA origami/ribbon structures were used rather than origami alone; but we have not quantified this effect nor explored its mechanism. (There are many possibilities—larger DNA nanostructures stick more strongly to mica, for example.)

DNA origami/ribbon template assembly and ligation. Short DNA strands were purchased from IDT DNA. Single-stranded M13mp18 bacteriophage DNA, T4 DNA Polynucleotide Kinase, and T4 DNA Ligase were purchased from New England Biolabs. DNA strands and buffers are mixed to obtain 50 μL of the following "assembly mixture". (Amounts of components are given as either the final concentration of that component, or the volume of that component added.)

1× TAE Mg^{2+} (12.5 mM Mg-acetate, 40 mM Tris-acetate, 1 mM EDTA, filtered with a 0.22 μm filter)
1×T4 DNA ligase buffer (50 mM Tris-HCl, 10 mM $MgCl_2$, 1 mM ATP, 10 mM Dithiothreitol)
10 nM M13mp18 bacteriophage DNA
50 nM of each origami staple
10 nM of each DNA ribbon adapter strand
100 nM of each zig-zag ribbon tile
3 μL T4 Polynucleotide Kinase

The above reaction mixture is placed in a 0.6 mL PCR tube and incubated using the following temperature profile:

1) 37°C for 1 hour
2) 65°C for 20 minutes
3) 90°C for 5 minutes
4) 90°C to 40°C at 1°C per 1 minute
5) 40°C to 25°C at 1°C per 1 hour

The assembly mixture is then diluted and mixed with additional components to form 500 μL of the following "ligation mixture":

1× TAE Mg^{2+}
1× T4 DNA ligase buffer
25 μL T4 DNA ligase
50 μL assembly mixture

Ligation is allowed to proceed in the above solution at room temperature for 12 to 24 hours.

Purification of DNA origami/ribbon templates. Assembled and ligated templates are separated from other reaction products using Millipore Microcon YM-100 spin filters (100 kD MWCO). 100 μL of the ligation mixture is gently mixed with 300 μL of sodium-based assembly buffer (0.75 M NaCl, 0.01 M Na_2HPO_4, pH ~8 at 25°C, 0.22 μm filtered) and transferred to a YM-100 spin filter according to the product's instructions. The filter is spun in an Eppendorf temperature-controlled centrifuge at

DOI: 10.1038/NNANO.2009.311

4°C and 1000 g for 12 min. 400 μL of assembly buffer is added to the retentate in the spin filter and gently mixed using a 1000 μL pipette. The filter is spun again at 4°C and 1000 g for 8 minutes. The retentate is then recovered according to the product's instructions. The recovery should yield about 100 μL of solution. (Note that the spin time for the second filtration can be adjusted to obtain approximately the desired volume). The recovered solution contains ~1 nM concentration of DNA templates in sodium buffer. We have found that without this buffer exchange, the presence of magnesium at millmolar concentrations causes precipitation of NL-SWNTs when DNA templates are later mixed with the NL-SWNTs. The elimination of free assembly components was verified using ND-PAGE analysis. (Origami/ribbons do not migrate in ND-PAGE gels, but excess staples which we are interested in measuring, do.) Ligated origami/ribbon templates remain stable in the sodium-based assembly buffer, as evidenced by subsequent AFM.

S3 Assembly of NL-SWNTs with origami-ribbon templates

We combined NL-SWNTs with origami-ribbon templates in two different types of experiments: (1) the binding of red NL-SWNTs or blue NL-SWNTs *independently* with origami-ribbon templates bearing cross patterns of red and blue hooks to measure the specificity of binding and fidelity of alignment to the hooks and (2) the binding of red NL-SWNTs and blue NL-SWNTS *simultaneously* with origami-ribbon templates bearing cross patterns of red and blue hooks to create cross-junctions. In both cases, the basic recipe (with amounts of components given as either the final concentration of that component, or the volume of that component added) for combining NL-SWNTs with origami-ribbon templates is the same:

$\sim$0.75 M NaCl
$\sim$0.01 M Na_2HPO_4
10 μL of purified DNA templates
0.5 to 3 μL of red NL-SWNTs
0.5 to 3 μL of blue NL-SWNTs

This mixture (pH $\sim$8) is kept at 25°C for 10 to 100 minutes and then deposited directly on the desired substrate for characterization. We have not systematically studied the kinetics but binding times between 30 and 35 minutes appear to give the best results under our conditions.

A couple comments:

1. Nanotubes probably attach to DNA templates via multiple hook-linker interactions, but the details of the attachment process remain uncertain. For example, multiple linkers could first attach to multiple DNA hooks via their toeholds before each hook-linker pair completes the branch migration process. Alternatively, branch migration could occur at a single attachment site followed by alignment via additional attachments. Further work is required to fully understand the attachment processes.

2. We do not have a direct method for quantifying the concentration of post-purification origami-ribbon templates and NL-SWNTs in the assembly solution. However, assuming every M13mp18 DNA strand results in an assembled template, and every template is retained durning purification, then we would have $\sim$0.5 nM of origami-ribbon templates in the assembly mixture. $7\mu\text{m}\times7\mu\text{m}$ topographic fluid mode AFM scans for origami/template/NL-SWNT constructs in experiments with a single type of tube (red or blue) typically show 2 to 3 SWNTs for every visible DNA template on the mica surface. Thus it is plausible (if binding rates of NL-SWNTs and templates to the mica are similar) that the concentration of NL-SWNTs could be in the low (say 1-2) nanomolar range.

DOI: 10.1038/NNANO.2009.311

S4 Atomic force microscopy of constructs under fluid

Deposition on mica substrates. After assembly, 5 μL of the assembly solution is added to a piece of freshly cleaved mica. Following this, a 40 μL drop of 1$\times$ TAE/Mg^{2+} was added on top. Finally, a 20 μL drop of 10 mM nickel (II) acetate (0.22 μm filtered) was added. The sample was then immediately imaged with an AFM. Fig. S5 shows examples of SWNT cross-junctions deposited on mica and imaged using tapping mode AFM under fluid. AFM characterization suggests that the asymmetry of the constructs may play a role in deposition. In the same experiments we used to measure the alignment of red or blue nanotubes to their respective hook arrays, we also counted the number of occurences of DNA origami/ribbon constructs with their red face down or blue face down:

	undecidable	blue face down	red face down	total
red tubes attached	16 (11%)	29 (19%)	106 (70%)	151
blue tubes attached	9 (8%)	14 (12%)	97 (80%)	120

There is a bias (70–80%, when 50% was expected) for an origami/ribbon construct to have its red face down and its blue face up, regardless of whether it is bound by a blue or a red tube. While the origami are symmetric at the coarse scale of their overall shape, they are highly asymmetric at a smaller length scale; almost all of the nicks in the phosphate backbone (except for at the row of blue hooks) of the origami we used fall on the red face of the origami. Thus one might expect that the origami can assume a configuration with the red face being convex much more easily that it can assume a configuration with the blue face being convex; if the red face is convex, the nicks can open and relieve strain, if the blue face is convex, no such strain relief can occur. Perhaps this plays a role in the asymmetric deposition rate. Further work will be required to confirm and understand this deposition effect.

Collection of alignment statistics using atomic force microscopy. To collect alignment data, we prepared DNA origami/ribbon templates with the cross-junction hook pattern. The templates were mixed with either red or blue NL-SWNTs *independently*, and annealed according to the standard procedure, and deposited on mica (as described above). A Veeco Multimode AFM with a Nanoscope IIIa controller was operated in tapping mode with a fluid cell. The imaging parameters were the same as described in (*30*). All images were collected at 512 $\times$ 512 pixel resolution using a scanning speed between 1.0 and 6.0 lines per second. A 10 μm $\times$10 μm or 7 μm $\times$7 μm area scan was first taken at a random location on mica. Every visible DNA template in that area was scanned in greater detail until the template quality, template orientation and SWNT alignment angle could be clearly established (usually requiring a 500 nm$\times$ 500 nm or smaller scan area).

S5 Electronic characterization of cross-junctions

Deposition of SWNT/DNA template constructs on SiO_2 substrates. A $\sim$ 1 cm $\times$ 1 cm piece of p-doped Silicon wafer with a thermally grown SiO_2 layer (300 nm or 1 μm) was cleaned with dichloroethane (DCE) and isopropanol (IPA) in an ultrasonicator bath. The wafer was then exposed to O_2 plasma in an Anatech SP100 plasma system (Anatech) at 80 W, 200 mTorr for 3 minutes. A 5 μL solution containing SWNT/DNA template constructs was then immediately deposited onto the wafer surface followed by a 7 μL drop of 10 mM Ni^{2+} acetate solution and 40 μL drop of 1$\times$ TAE/Mg^{2+}. After 1 hour of incubation at room temperature, excess salt residue was washed away using 0.1 M ammonium acetate, (pH 6 at 25°C). The wafer was dried using compressed nitrogen gas. Deposited SWNT/DNA template constructs could then be imaged by tapping mode AFM on the dry silicon substrate (Fig. S6) and by scanning electron microscope (SEM) albeit with lower resolution. Although the ribbons on DNA templates appeared twisted and folded and under dry mode AFM, cross-junction geometry of SWNTs was typically intact (Fig. S6). Within a 400 μm^2 area of the silicon wafer, we typically found 5 to 10 self-assembled SWNT cross-junctions.

Lithographic fabrication of contacts to the SWNT cross-junctions. Positions of self-assembled SWNT cross-junctions are located on the Si/SiO_2 substrate, with respect to the pre-fabricated reference markers, using an AFM. Standard electron-beam lithography techniques are employed to make electrical contacts to the nanotubes. Briefly, a bi-layer resist consisting of 250 nm LOR 3B lift-off resist (MicroChem, baked at 190°C for 1–3 minutes) and 150 nm PMMA C2 (MicroChem, baked at 160°C for 10–15 minutes) are spun on the sample. Electrode patterns are written using a Quanta 200F (FEI tools) equipped with nanometer pattern generation system (NPGS). After the development of the resist, the sample is rinsed in "DNA AWAY" (Molecular BioProducts) for 6 seconds, washed with DI water, rinsed with HCl for 6 seconds and washed again with DI water. The rinsing steps have three purpose: first, to prime the surface (HCl has been shown to improve the hydrophilic nature of the silicates by hydrolyzing them, therefore, priming the metal wetting properties of the substrate surface), second, to degrade substrate bound DNA so that it does not adversely affect the adhesion of metal electrodes to the substrate and third, to remove DNA from NL-SWNTs at contact regions so that it does not adversely affect the metal-SWNT junction. (Note that at this point in the process, NL-SWNTs near the cross-junction and DNA templates are presumably protected from the rinses by resist. However, we found that we could not resolve the DNA templates by AFM post-liftoff.) We do not know whether the DNA on the NL-SWNTs in the contact regions is fully degraded or whether the residue of degraded DNA is washed away. However, NL-SWNTs treated in this manner exhibit better conductivity, presumably due to better electrode-nanotube contact. Electrodes are then thermally evaporated via e-beam evaporator (Temescal BJD 1800). Each electrode has $\sim$5 nm thick Pd layer contacting the SWNT and and 40 nm Au layer protecting the Pd contact. (Palladium was chosen over gold or chromium because palladium has better wetting properties than gold and it has been shown to produce a smaller Schottky barrier at contacts with SWNT than does chromium because its work function better matches that of carbon nanotubes. Further, we chose not to apply a standard high temperature annealing protocol [*e.g.* 600°C for 30 minutes under argon] in attempt to preserve the DNA templates.) Finished devices are shown in Fig. 3 and supplementary Figs. S8 and S9.

After the resist lift-off process, the device is mounted in a chip holder and electrical contact between the bonding pads and holder are made using a wire bonder. The chip holder is inserted in a socket connected to our measuring setup.

DOI: 10.1038/NNANO.2009.311

In all, we attempted fabrication on 23 cross-junctions. Of these, six had measurable conductance in one or both nanotubes, three had field effect transistor (FET) like behavior. Of the three FET-like devices, one had stable properties throughout the period of measurement.

Device characterization. All devices were characterized using similar procedures. Figs. 3 and S8 show the measurement setup and results of the stable FET-like device (giving similar results over tens of measurements). Fig. S9 shows the measurement setup and results for an additional FET-like device, which was short-lived (providing just the three sweeps in Fig. 9).

Outputs from a digital-to-analog converter (DAC) card (National instruments) in a PC were used to maintain voltages between different electrodes. Currents were measured via a current pre-amplifier which also served as a virtual ground. Our four-electrode setup allowed us to measure each SWNT independently and determine its room temperature properties. In general, for a given device, we first measured the two terminal current flow across each nanotube as a function of voltage (the other nanotube is left floating) to see if good contacts had been made. Then IV curves were measured as a function of back-gate voltage to determine if the SWNT was metallic or semiconducting (except in cases where the back-gate failed, as in the case of the stable device). Based on these IV curves (and if there was potential for FET-type behavior) we chose one SWNT as the channel, and the other as the gate channel, and assigned the four electrodes as source (S), drain (D), gate (G) and auxiliary gate (g) electrodes. After picking the channel and gate nanotubes, we then measured the inter-nanotube tunneling current as a function of applied gate voltage. Using this data, we pick a suitable range of gating voltage V_G and measure (a) I_{SD} at fixed V_{SD} as a function of V_G and (b) I_{SD} at fixed V_G as a function of V_{SD}. During these measurements, one terminal of the gate SWNT (G) is connected to the applied voltage while the other terminal (g) is left floating. To protect the device from the gate's insulating layer breakdown etc., the voltage, V_G, is applied through a 100 MΩ resistor which, along with the gate capacitance, acts as a low-pass filter.

In particular, Fig. 3 shows the stable device and its function as a FET; S8 shows more detailed data on its electronic properties. Two electrode measurements across each SWNT suggested that one SWNT (from source electrode S to drain electrode D) was a p-type semiconductor and the other SWNT (from gate electrode G to auxillary electrode g) was either metallic or semiconducting. (For this particular device, the back-gate was not functioning.) We chose the SWNT across electrodes S and D to be the conducting channel due the much lower apparent resistance of that channel (∼2 MΩ, see Fig. 8). The SWNT across electrodes G and g was chosen to be the gate channel due to that channel's high resistance (∼6 GΩ channel resistance, see Fig. 8b). However, the inter-nanotube current measurement between electrodes G and D indicates that the resistance (∼3 MΩ resistance for $V_{GD} < -0.5\,V$, Fig. 8c) through the gate nanotube and electrode G (where the gating voltage is applied) may be far lower than 1 GΩ at negative gate voltages.

Measurement of the inter-nanotube tunneling current (Fig. S8c) also shows an insulating region between $V_{GD} \sim -0.5$ V to 0.5 V. This could be due to insulation by DNA or other organic residue or an inter-nanotube Schottkey barrier. We chose to sweep V_{GD} in this range to characterize FET-type gating of the current channel and confirmed the identity of the blue SWNT as a p-type semiconductor.

The gate electrode G is in close proximity (∼70 nm) to the conduction channel SWNT and may contribute to the current switching behavior shown in Fig. 8d. Further experiments are needed to understand the field effect gating mechanism and to decouple the contribution of the SWNT gate from that of gate electrode.

S6 Open questions.

The protocols described in this paper describe sufficient conditions for the creation of SWNT cross-junction devices. However, there remain open questions concerning what the simplest necessary procedure for creating cross-junction devices might be, as well as what parts of the protocol are most important for success:

1. *LNA versus DNA toeholds*. We have found that, under the conditions reported above, 5 nucleotide LNA toeholds give good results. We have been unable to find conditions under which 7 and 8 nucleotide DNA toeholds give good results; they resulted in cross-linking of SWNTs or aggregation. For some experiments, 5 nucleotide DNA toeholds were used and SWNT-origami binding and alignment was observed but with poor yield. However, conditions and sequences for the use of 5 nucleotide DNA toeholds were not optimized and so conditions under which less expensive, short, DNA toeholds (5 or 6 nucleotides) give good yields of cross-junctions may be found. In addition to its role as a stronger binding toehold, LNA may also be advantageous in this system because its constrained backbone may give it a lower intrinsic affinity for SWNTs; this idea has also not been tested.

2. *Plain origami versus origami with ribbons*. The use of ribbons with DNA origami appeared to increase the yield of observed structures. However we have not rigorously quantified this effect, and we have obtained some aligned SWNTs and cross-junctions on origami alone. Other protocols may be better suited for the use of DNA origami alone, for example the deposition of DNA origami on surfaces before their assembly with SWNTs.

3. *Hooks with versus hooks without poly-T segments. Yield and alignment as a function of flexibility.* We added poly-T segments between staples and hooks with the idea that they would facilitate SWNT alignment by acting as joints or spacers. However, we did not test the efficacy of assembly without poly-T segments. This is part of a larger set of questions about the degree of alignment as a function of hook spacing, linker length, and hook length. The effects of such variables on the quality of alignment are not understood.

4. *Schemes using strand displacement versus other protected schemes without strand displacement*. Here we use a protection strands to prevent the labeling domain from binding to the SWNT to which it is attached (via the linker domain) or from cross-linking this SWNT with other SWNTs. The 5-nucleotide toehold is available for binding the hook and initiation of strand displacement. The question is whether toehold binding to the hook is itself sufficient to align a SWNT on an origami (since multiple toeholds can bind an origami at once). Initial experiments using hooks that are composed of only the 5 nucleotide sequence complementary to the toehold (and are thus incapable of displacing the protection strand by branch migration) indicated that binding and alignment can occur without a complete 20 nucleotide labeling domain but these experiments have not been optimized or compared quantitatively to results with the full labeling domain. Note that in these experiments with short hooks, the protection strand and duplex domain in the linker complex remain intact—thus while displacement of the protection strand may not be necessary, the rigid duplex it forms may be important in holding the toehold away from the SWNT.

5. *SWNT alignment as a function of NL-SWNT purity.* While preparations of NL-SWNTs with ratios of free linker to bound linker as high as ~1:3 gave good alignment of NL-SWNTs to origami templates, NL-SWNTs with a lower amount of free linker might give still better results, since free

DOI: 10.1038/NNANO.2009.311

linkers presumably bind hooks on DNA origami and render them ineffective as binding sites for NL-SWNTs.

6. *Why are the ends of nanotubes so often flush with the edges of DNA origami?* In perhaps 25% of cases nanotubes bind their complementary hook arrays so that one end of the nanotube is at the end of a hook array. It will be interesting to know how statistically significant this effect is, and if it is a real effect, what is the the mechanism behind it. There are many instances where it would be desirable to have nanotube ends meet rather than having nanotubes cross and so harnessing the effect could be very useful.

7. *What is the detailed structure of the linkers on the SWNT and how does this affect alignment?* It is unclear what the density of the linkers are on the NL-SWNTs, whether they close packed or have gaps, whether their dispersal domains wrap the SWNTs helically or not, whether the linkers dynamically rearrange on the SWNT surface or not, what the number of labels available for binding hooks is, or how any of these variables ultimately effect the alignment of SWNTs on DNA origami.

8. *What is the nature of the barrier between SWNTs in our system? Can the intervening DNA layer act as a dielectric?* So far, the effect of the DNA linkers and DNA origami template between carbon nanotubes is unclear. In the device best studied, AFM showed no residual origami template at the junction and other explanations for the observed barrier (e.g. a Schottkey barrier) are possible. However, DNA residue from the origami may have remained between the tubes, and the SWNTs were themselves coated with DNA linker complex. Lithographic steps to add metal electrodes left visible DNA in some cases; this suggests that fabrication might be optimized to leave behind origami templates. An important geometry to test is that of crossed carbon nanotubes bound to the same side of the origami (which, in principle, should not be difficult to synthesize) that should have less DNA between them (only the DNA linkers) and should thus exhibit a different distribution of device characteristics than the case with crossed carbon nanotubes on opposite sides of the origami. An important control will be devices that have been intentionally stripped of DNA. Improvements in locating and wiring up devices seem necessary to collect enough device data to address this question.

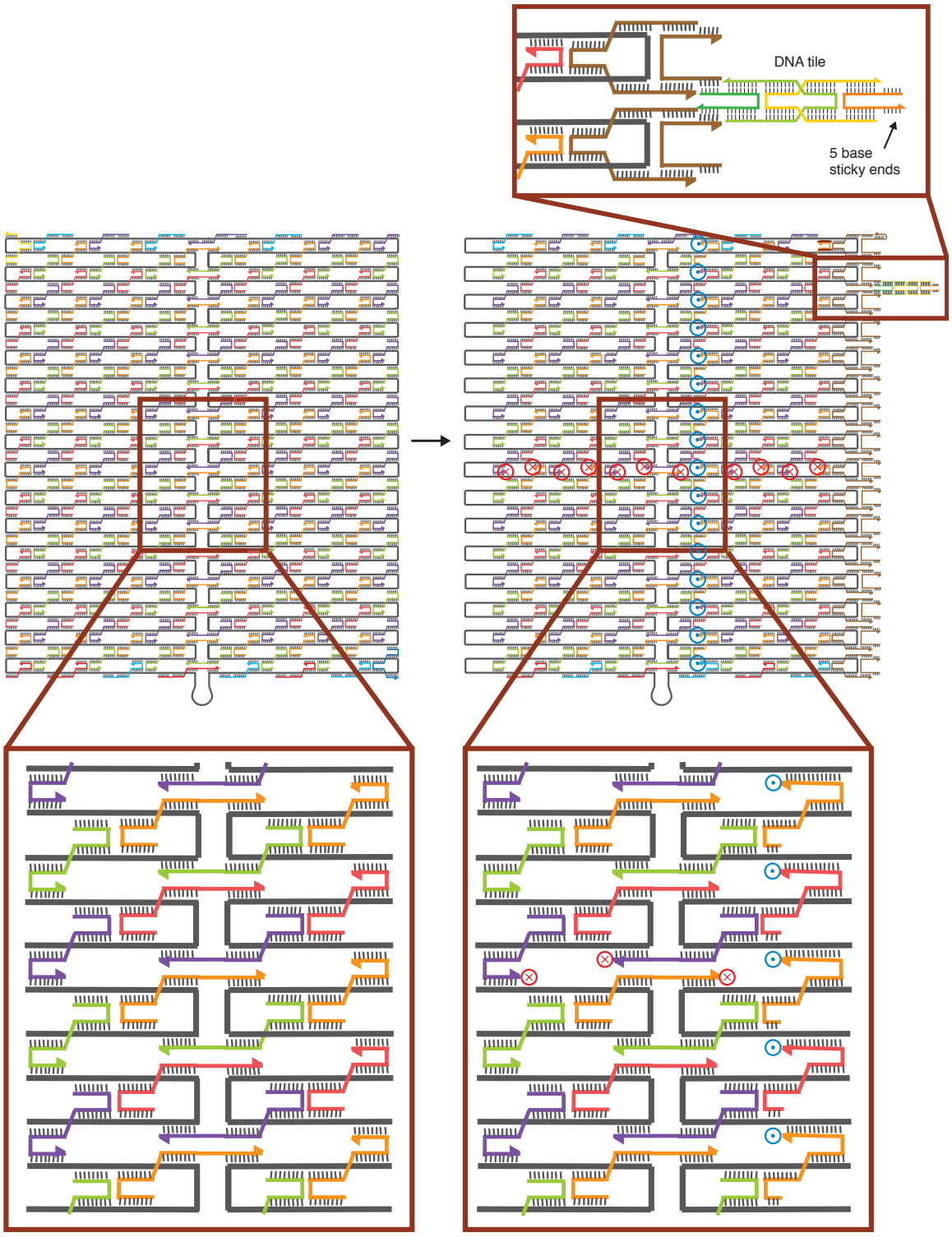

Figure S1: A schematic for the original "tall rectangle origami" (Supplementary Figs. S35 and S48 in (*20*)) is compared with a schematic of the modified rectangle origami we used as a template, at right. In our new design the leftmost column of staples was removed to decrease origami aggregation. The rightmost column of staples was replaced with tile adapter strands (Fig. S2 and S3) for nucleating zig-zag DNA ribbon growth. Blue dotted circles indicate blue DNA hooks extending out of the page. Red crossed circles indicate red DNA hooks extending into the page.

DOI: 10.1038/NNANO.2009.311

Plate position	Position and sequence	Sequence
B1	t-5r18e-FHook1	5' - TATATTTTCATACAGGCAAGGCAAAGCTATATTTTTTGTCGGCAAGACCTCGCAAC - 3'
C1	t-3r18e-FHook1	5' - CAACGCAAAGCAATAAAGCCTCAGGATACATTTTTTTGTCGGCAAGACCTCGCAAC - 3'
D1	t-1r18e-FHook1	5' - CTGTAATAGGTTGTACCAAAAACACAAATATATTTTTGTCGGCAAGACCTCGCAAC - 3'
E1	t3r18e-FHook1	5' - TATGTAAAGAAATACCGACCGTGTTAAAGCCATTTTTGTCGGCAAGACCTCGCAAC - 3'
F1	t5r18e-FHook1	5' - TAACCTCCAATAAGAATAAACACCTATCATATTTTTTGTCGGCAAGACCTCGCAAC - 3'
G1	t-5r16f-FHook1	5' - ATATAATGGGGGCGCGAGCTGAAATTAACATCTTTTTGTCGGCAAGACCTCGCAAC - 3'
H1	t-3r16f-FHook1	5' - TGCAACTAGGTCAATAACCTGTTTAGAATTAGTTTTTGTCGGCAAGACCTCGCAAC - 3'
A2	t-1r16f-FHook1	5' - TCCATATATTTAGTTTGACCATTAAGCATAAATTTTTGTCGGCAAGACCTCGCAAC - 3'
B2	t1r16f-FHook1	5' - AGAGGCATACAACGCCAACATGTATCTGCGAATTTTTGTCGGCAAGACCTCGCAAC - 3'
C2	t3r16f-FHook1	5' - TAAAGTACCAGTAGGGCTTAATTGCTAAATTTTTTTTGTCGGCAAGACCTCGCAAC - 3'
D2	t5r16f-FHook1	5' - CCAGACGACAAATTCTTACCAGTAGATAAATATTTTTGTCGGCAAGACCTCGCAAC - 3'

Figure S2: The modified staples used to display the red ssDNA hooks.

Plate position	Position and sequence	Sequence
A7	t1r0g-FHook2	5' - TGATATAAGTATAGCCCGGAATAGGTG - 3'
B7	t1r2e-FHook2	5' - GTCGGTAATAAGTTTTAACCCGTCGAGAGGGTTTTTCATCCTAACCAGCCCCGTAT - 3'
C7	t1r4e-FHook2	5' - GAGACCCTCAGAACCGCCACGTTCCAGTAAGCTTTTCATCCTAACCAGCCCCGTAT - 3'
D7	t1r6e-FHook2	5' - GAGGTAGCACCATTACCATATCACCGGAACCATTTTCATCCTAACCAGCCCCGTAT - 3'
E7	t1r8e-FHook2	5' - ACGTAAAGGTGGCAACATACCGTCACCGACTTTTTTCATCCTAACCAGCCCCGTAT - 3'
F7	t1r10e-FHook2	5' - AAAGATAACCCACAAGAATAAGACTCCTTATTTTTTCATCCTAACCAGCCCCGTAT - 3'
G7	t1r12e-FHook2	5' - TGCACGCTAACGAGCGTCTGAACACCCTGAACTTTTCATCCTAACCAGCCCCGTAT - 3'
H7	t1r14e-FHook2	5' - CTGACCAAGTACCGCACTCTTAGTTGCTATTTTTTTCATCCTAACCAGCCCCGTAT - 3'
A8	t1r16e-FHook2	5' - TTATTTCGAGCCAGTAATAAATCAATAATCGGTTTTCATCCTAACCAGCCCCGTAT - 3'
B8	t1r18e-FHook2	5' - GAAAATTTCATCTTCTGACAGAATCGCCATATTTTTCATCCTAACCAGCCCCGTAT - 3'
C8	t1r20e-FHook2	5' - AATCGTCGCTATTAATTAAATCGCAAGACAAATTTTCATCCTAACCAGCCCCGTAT - 3'
D8	t1r22e-FHook2	5' - CGTTCGGGAGAAACAATAACAGTACATAAATCTTTTCATCCTAACCAGCCCCGTAT - 3'
E8	t1r24e-FHook2	5' - AATGAACAAAGAAACCACCTTTTCAGGTTTAATTTTCATCCTAACCAGCCCCGTAT - 3'
F8	t1r26e-FHook2	5' - GCAAATCAATATCTGGTCACCCGAACGTTATTTTTTCATCCTAACCAGCCCCGTAT - 3'
G8	t1r28e-FHook2	5' -CAGATACGTGGCACAGACATGAAAAATCTAAATTTTCATCCTAACCAGCCCCGTAT - 3'
H8	t1r30e-FHook2	5' - AGCCCTGAGTAGAAGAACTACATTCTGGCCAATTTTCATCCTAACCAGCCCCGTAT - 3'
A9	t1r32h-FHook2	5'-TACAGGGCGCGTACTATGGTTGCTAATTAACCGTTGTTTTTCATCCTAACCAGCCCCGTAT-3'

Figure S3: The modified staples used to display the blue ssDNA hooks.

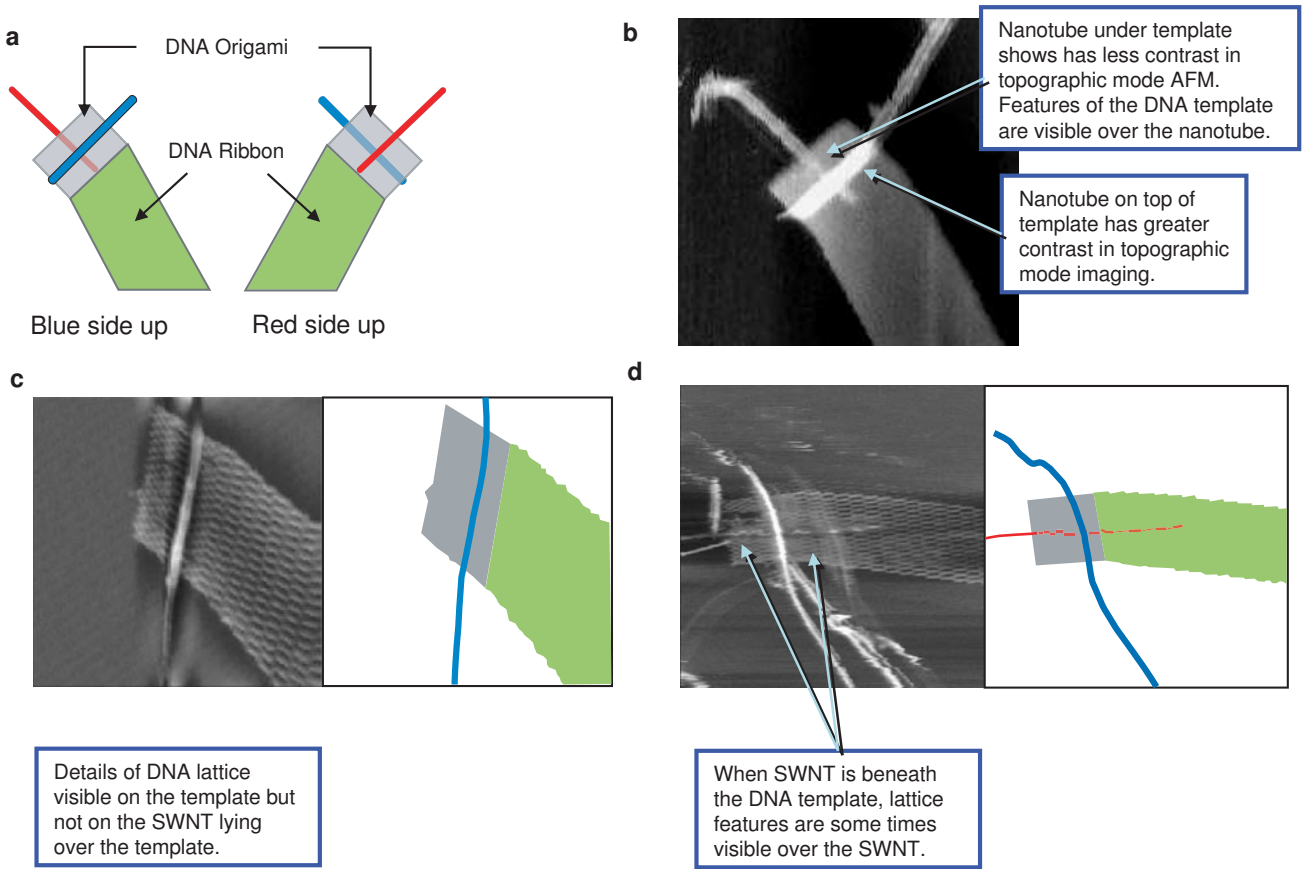

Figure S4: Understanding the orientation of SWNT/origami/ribbon constructs. **(a)** Origami/ribbon constructs have a handedness that allows one to distinguish which face of the origami is facing up, and which is facing down on the substrate. This allows the relative orientation of a SWNT and an origami to be measured over a 180° range rather than the 90° range possible if the origamis were used alone, without further markings. (It turns out that the alignment distributions we measure are roughly symmetric about their peak, and so in the end it would not have changed the conclusions of the alignment data, but this might have not been the case.) **(b)** Another cue which aids in understanding the structure of the cross-junctions is the topograhic height constrast of the two different nanotubes. In general the nanotube under the template images with lower height contrast than the nanotube on top of the origami. **(c)** and **(d)** Still a third cue is the "texture" of the carbon nanotube. Nanotubes that are apparently on top of the origami have a smooth (yet noisy) texture do the blue nanotubes in (c) and (d). When imaged with very high resolution, nanotubes apparently underneath the origami sometimes have a dashed or periodic appearance that seems correlated to the fine periodic structure of the origami or the ribbon, as does the red tube in (d). AFM height contrast and the texture of the nanotube are secondary cues as to the position (over or under the origami) of the nanotubes. They are not always observed but when observed are typically consistent with the position derived by the orientation of the origami/ribbon. Rarely they disagree—this may indicate nonspecific binding of blue tubes to red hooks or red tubes to blue hooks, which may explain some of the few nanotubes that have an incorrect orientation in the alignment distributions in Fig. 2.

DOI: 10.1038/NNANO.2009.311

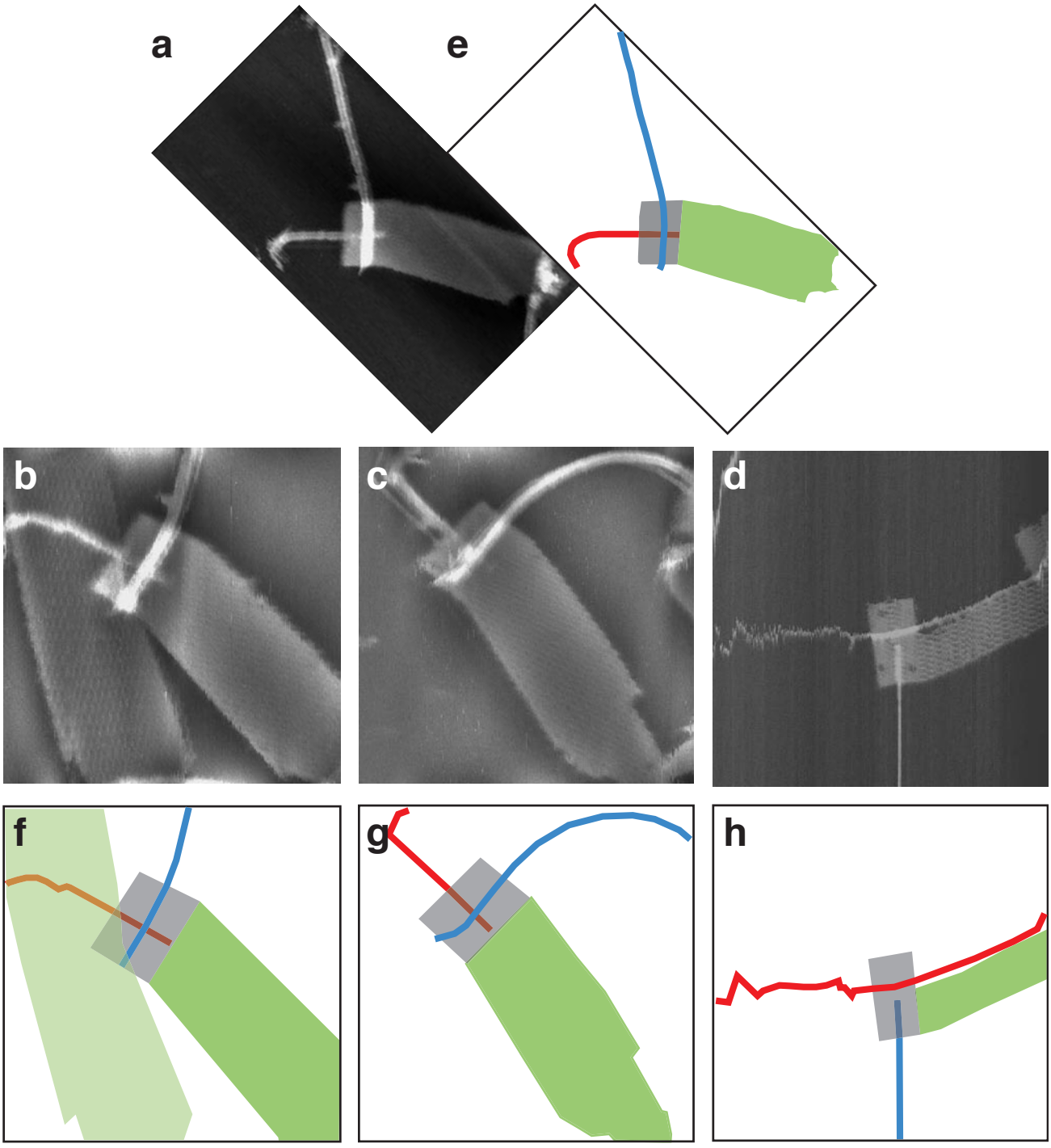

Figure S 5: **(a)–(d)** Topographic tapping mode AFM images of the self-assembled SWNT cross-junction deposited on a mica substrate and kept under fluid. (a)–(c) show cross-junctions on origami attached to 16-wide tile-wide ribbons. (d) shows a cross-junction on an origami attached to an 8-tile wide ribbon. The blue nanotube is under the origami according to the ribbon orientation; this is consistent with the faint details of the origami fine structure that may be seen on top of it. **(e)–(h)** Interpretations of (a)–(d). Red and blue SWNT are indicated, origami are gray, and ribbons are green. SWNTs that apparently run origami under or ribbons have had their color deemphasized. In (f) a ribbon that has fallen on top of part of the origami and red SWNT is represented in light green. (Details of the light green ribbon can clearly be seen in the AFM coincident with the red nanotube, which is why we interpret it as being on top of the red SWNT.)

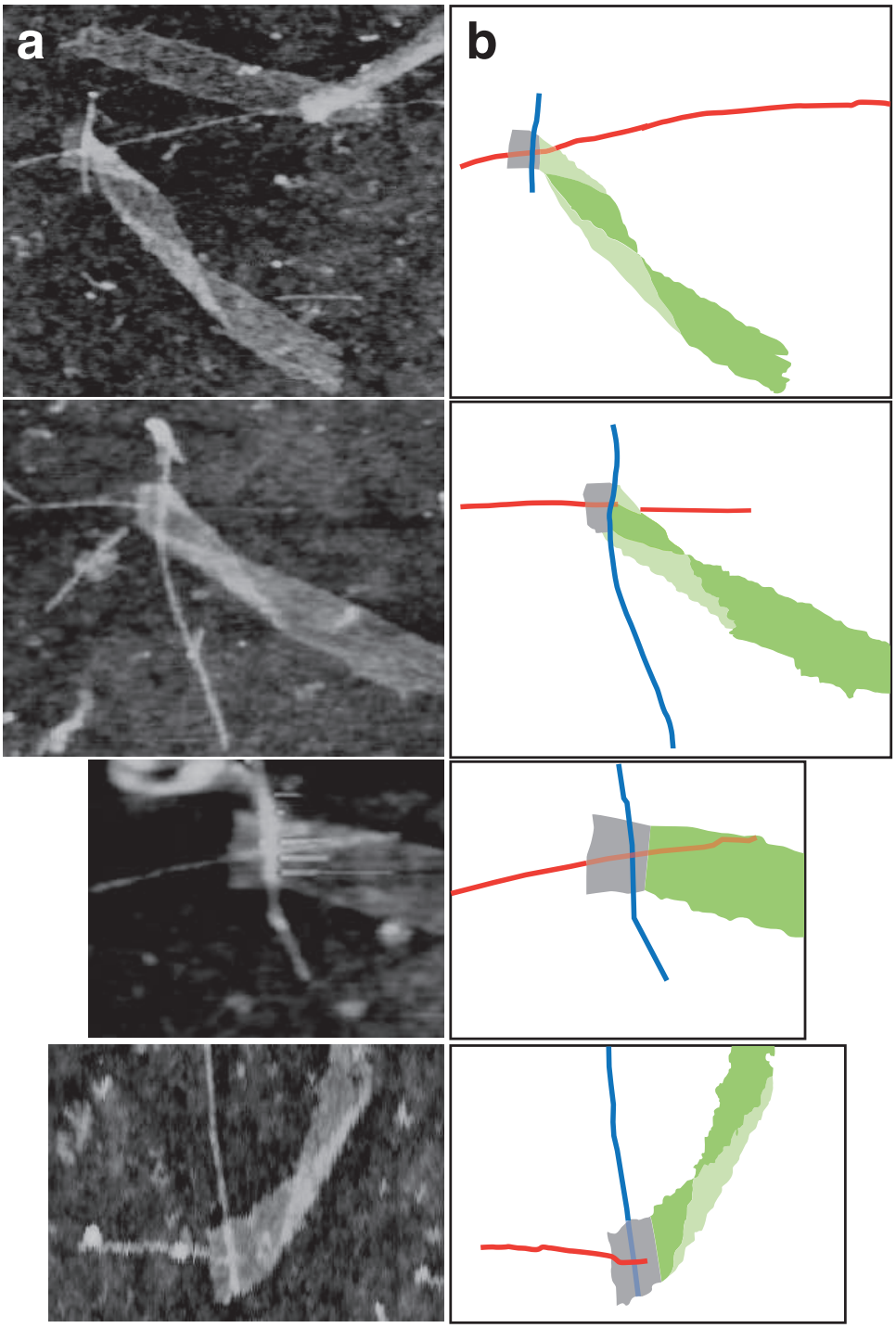

Figure S6: **(a)** topographic AFM images of the self-assembled SWNT cross-junctions deposited on a silicon substrate. The image is taken on a dry substrate in tapping mode. The width of the ribbons is ~100 nm. **(b)** interpretations of the AFM images in (a). Blue and red SWNT are indicated. Origami are indicated in gray, the ribbon in dark green, and places where the ribbon folds on itself to give a double-width ribbon are in light green. Contours for DNA structures are subjective, it is difficult to tell in these images where the origami ends and the ribbon begins. SWNTs that apparently run under origami or ribbons have had their color deemphasized. For the bottom cross-junction, the position of the blue and red nanotubes (over or underneath the origami), as derived from the ribbon orientation and as suggested by which tube has the greater height contrast are in conflict (see S4). We have interpreted the image as though the ribbon-orientation tells the correct position, but this ribbon is so distorted that perhaps it has been "bent up" in a way that makes its apparent handedness incorrect.

DOI: 10.1038/NNANO.2009.311

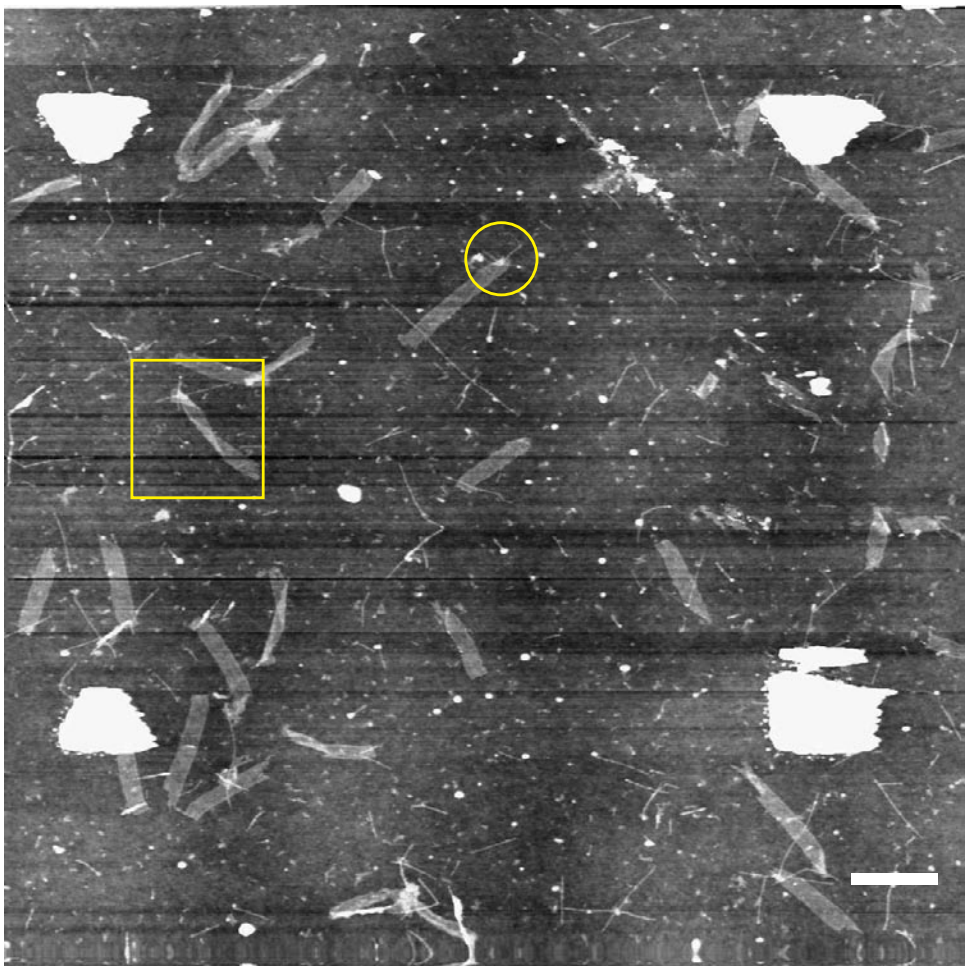

Figure S7: A typical wide-field view of cross-junctions on silicon. Two cross-junctions are outlined in yellow. In this particular wide-field view roughly 35 distinct DNA structures can be identified. 17 have identifiable origami and ribbon domains. Of these 12 have one or more SWNTs associated with the origami, and of these two have geometry judged to form a cross-junction. The boxed area contains the cross-junction shown at the top of Supplementary Fig. S6. The yield of DNA-templated cross-junctions is not greater, per unit area, than the number of crosses created by randomly associating SWNTs (perhaps a few here). Our measurement of the alignment of SWNTs to the lines of hooks on the origami (Fig. 2), as well as the relative sparsity of individual SWNT/SWNT crosses on ribbons in this image, suggest that the individual SWNT/SWNT crosses associated with the origami in this image are the result of specific binding rather than random association. Scale bar 500 nm. ~500 nm white features are gold alignment markers.

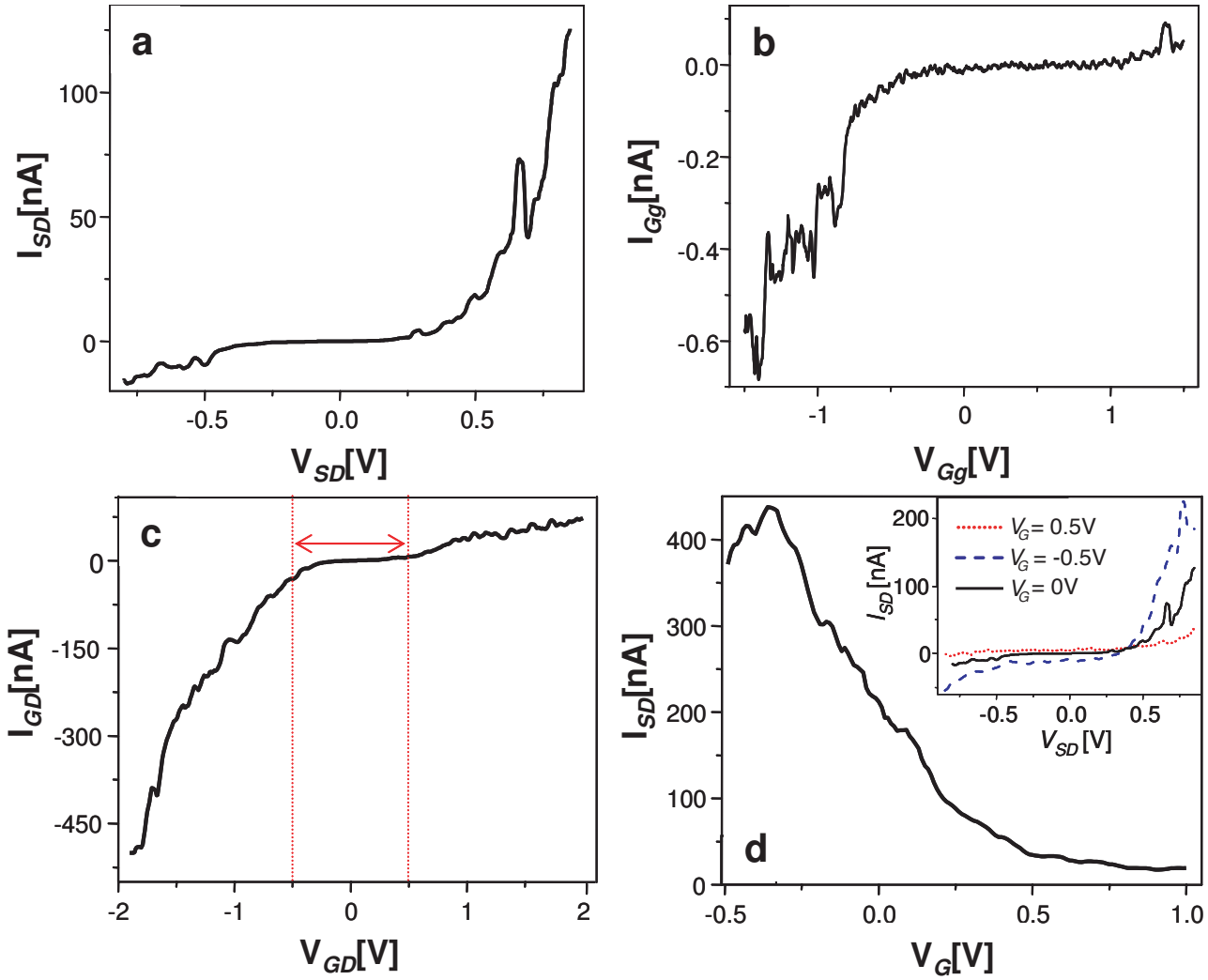

Figure S 8: Electrical characterization of the self-assembled SWNT cross-junction in shown Fig. 3. For this particular device, the back-gate was not functioning. **(a)** Electrical measurement for the blue SWNT (source electrode S and drain electrode D) showing a nonlinear behavior suggestive of a p-type semiconductor. **(b)** Electrical measurement for the red SWNT (across gate electrode G and auxillary electrode g) showing high resistance. Lack of a back-gate meant that it was not possible to identity the red SWNT definitively as a metallic or semiconducting. The apparent bad contact g may be responsible for its nonlinear behavior. **(c)** The inter-tube conductance as measured between electrode G and D. The red arrow marks the insulating region where there is little current leakage between the SWNTs. **(d)** Source-drain current (electrodes S and D) versus SWNT gate voltage (electrode G) for source-drain bias of 0.85 V. Gating of the blue SWNT confirms it as a p-type semiconductor. The inset shows the source-drain I-V for different SWNT gate biases.

DOI: 10.1038/NNANO.2009.311

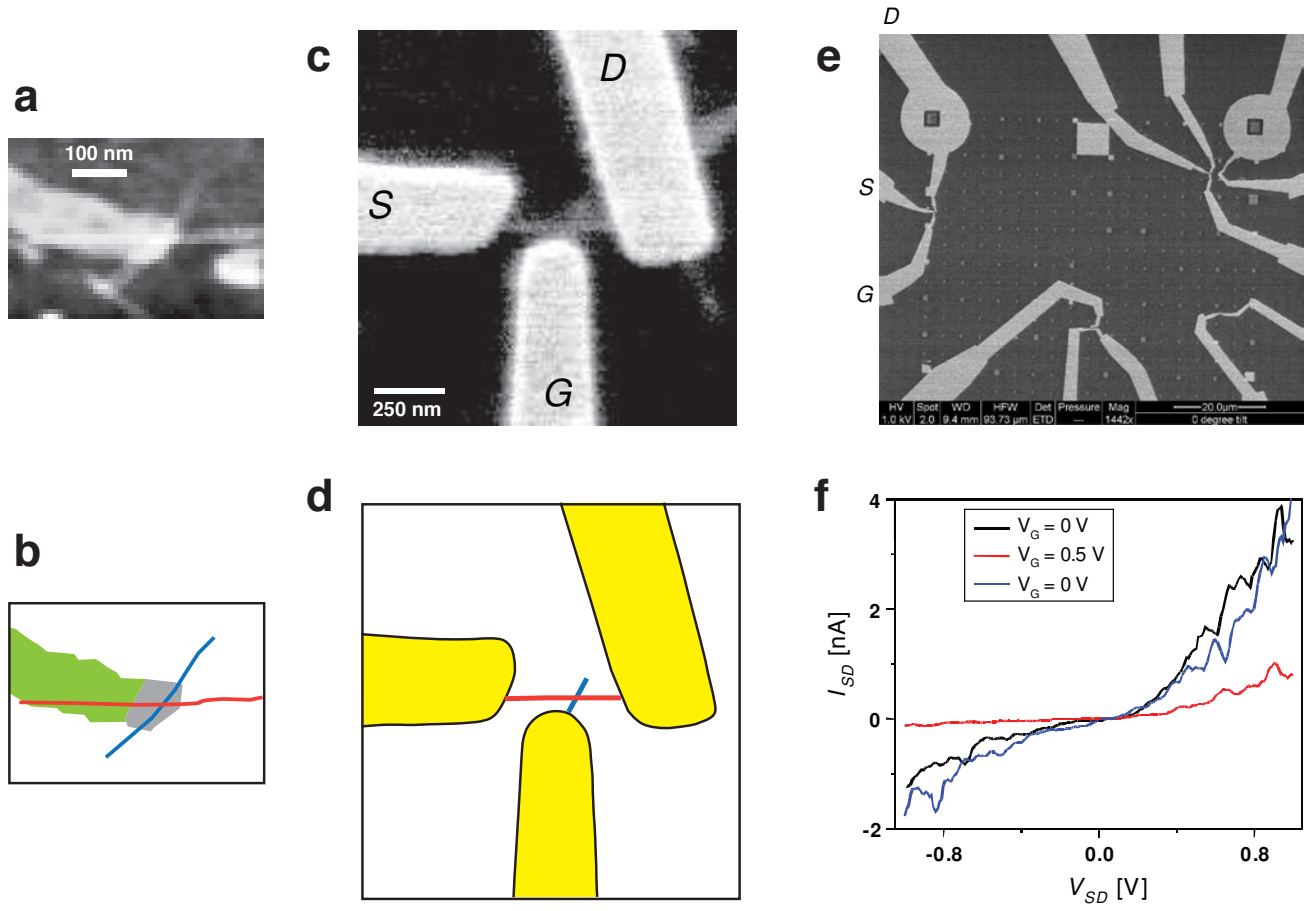

Figure S9: Electrical measurement of a second SWNT cross-junction exhibiting FET-type behavior, although it was only short-lived. **(a)** Dry mode AFM of the SWNT cross-junction on silicon before deposition of electrodes. **(b)** Interpretation of (a) showing red and blue SWNT as well as origami (gray) and ribbon (green). Orientation of the ribbon is uncertain and other cues are not present so it is impossible to tell which SWNT is on top. **(c)** Scanning electron micrograph (SEM) of the device after Pd/Au electrode deposition. **(d)** Interpretation of (c) indicating red and blue SWNTs. The DNA template is not clearly visible and may not be present after electrode fabrication. **e** SEM of large field showing electrodes short-lived device, alignment marks, and a variety of contacts to other devices. **(f)** Electrical measurement of gate-dependent switching of a resistive red SWNT, where the blue SWNT is used as the gate. A constant back gate voltage of 10 V is used for this measurement. Observed switching behavior was limited to just these few sweeps.